Spin state of iron in Fe_{3}O_{4} magnetite and h-Fe_{3}O_{4}

Amelia Bengtson, Dane Morgan, and Udo Becker

1   <u>Title:</u> Spin state of iron in Fe_3O_4 magnetite and h-Fe_3O_4
2
3   <u>Authors:</u> Amelia Bengtson[1,2], Dane Morgan[1], Udo Becker[2]

4   [1] University of Wisconsin-Madison, Department of Materials Science & Engineering
5   [2] University of Michigan, Department of Earth and Environmental Sciences
6
7
8   <u>Corresponding Author:</u>
9   Amelia Bengtson
10   Materials Science and Engineering Department
11   University of Wisconsin-Madison
12   1509 University Avenue
13   Madison, WI 53706-1595
14   Fax: 608/262-8353
15   e-mail: akbengtson@wisc.edu
16
17

18

20

21 **Abstract**

22 The high-pressure behavior of magnetite has been widely debated in the literature. Experimental
23 measurements have found conflicting high-pressure transitions: a charge reordering in magnetite from
24 inverse to normal spinel [Pasternak, M.P., et al. J. Phys. Chem. Solids **65**, 1531 (2004); Rozenberg, G.K.,
25 et al. PRB. **75** (2007)], iron high- to intermediate-spin transition in magnetite [Ding, Y., et al. PRL **100**
26 (2008)], electron delocalization in magnetite [Baudelet, F., et al. PRB **82** (2010); Glazyrin, K., et al. Am.
27 Min. **97**, 128], and a structural phase transition from magnetite to h-Fe_3O_4 [Dubrovinsky, L.S., J. Phys.:
28 Condens. Matter **15**, 7697 (2003); Fei, Y.W., Am. Min. **84**, 203 (1999); Haavik, C., Am. Min. **85**, 514
29 (2000)]. We present the first *ab initio* calculations of iron's spin state in magnetite and h-Fe_3O_4, which
30 helps resolve the high-pressure debate. The results of the calculations find that iron remains high spin in
31 both magnetite and *h*-Fe_3O_4; intermediate-spin Fe is not stable. In addition, magnetite remains inverse
32 spinel but undergoes a phase transition to *h*-Fe_3O_4 near 10 GPa. Magnetite has a complex magnetic
33 ordering, multiple valence states (Fe^{2+} and Fe^{3+}), charge ordering, and different local Fe site
34 environments, all of which were accounted for in the calculations. The lack of intermediate-spin iron in
35 magnetite helps resolve the spin state of Fe in perovskite, the major mineral in the lower mantle. In both
36 magnetite and perovskite, XES measurements in the literature show a drop in satellite peak intensity by
37 approximately half, which is interpreted as intermediate-spin Fe. In both minerals, calculations give no
38 indication of intermediate-spin iron and predict high-spin iron to be stable for defect-free crystals. The
39 results question the interpretation of a non-zero drop in XES satellite peak intensities as intermediate-spin
40 Fe.
41

42

43
44

I. INTRODUCTION

45

46   Magnetite (Fe_3O_4) has been of interest throughout history because it is one of the most magnetic

47   naturally-occurring minerals and is important for paleomagnetic measurements and past continent

48   reconstruction[1]. Magnetite can also be found at higher pressures in the mantle wedge of subduction zones

49   [2] formed as a by-product of serpentinization of olivine [3]. In addition, electrical resistivity measurements

50   in magnetite are useful for interpreting magnetotelluric measurements of the mantle [4].

51   The high-pressure structural, electronic, and magnetic properties of Fe_3O_4 are not well

52   characterized and the complex coupling of Fe spins contributes to these properties. Changes in magnetic,

53   spin, and structural states will alter density, elasticity, and electrical conductivity [5] and thus have an

54   influence on interpretation of magnetotelluric measurements. In addition, changes that occur in the

55   electronic or magnetic structure of Fe_3O_4 at high-pressure could reset magnetic ordering in meteorites that

56   collide at high-pressure, therefore complicating the interpretation of paleomagnetic data [6].

57   Fe_3O_4 has recently been suggested to undergo a transition to an intermediate-spin state on some of

58   the Fe atoms[7]. The nature of the possible intermediate-spin transition in magnetite is important both for

59   understanding Fe_3O_4 and for a more general understanding of the spin state of Fe in the Earth's lower

60   mantle. Despite numerous experimental measurements and theoretical calculations, the spin state of Fe in

61   perovskite, the dominant mineral in the lower mantle, is still under debate. X-ray emission spectroscopy

62   (XES) measurements find the satellite peak intensity of Fe in perovskite drops to a non-zero value with

63   increasing pressure, which is interpreted as a transition from high- to intermediate-spin Fe[8]. However,

64   theoretical calculations do not support intermediate-spin Fe in perovskite [9,10-13]. XES measurements in

65   magnetite show a similar drop in satellite peak intensity to perovskite, suggesting the spin state of Fe in

66   magnetite is also intermediate-spin[7]. Calculations of the spin state of Fe in magnetite will therefore

67   provide additional evidence to help settle the more general debate over whether intermediate-spin Fe is

68   occurring in high-pressure Fe compounds.

69   At ambient pressure and temperature, magnetite has an inverse spinel structure

70 $\left[Fe^{3+}\right]_{TET}\left[Fe^{2+/3+}Fe^{2+/3+}\right]_{OCT}$ with a random distribution of Fe^{2+} and Fe^{3+} on the octahedral site [14]. The

71 charges average to an effective valence state of $Fe^{2.5+}$ on the octahedral sites. In the literature, agreement

72 exists that a transition occurs in Fe_3O_4 between 10-20 GPa, but there is lack of agreement as to the type of

73 transition. ^{57}Fe Mössbauer spectroscopy measurements suggest the high-pressure phase goes through an

74 inverse- $\left[Fe^{3+}\right]_{TET}\left[Fe^{2+/3+}Fe^{2+/3+}\right]_{OCT}$ to normal- $\left[Fe^{2+}\right]_{TET}\left[Fe^{3+}Fe^{3+}\right]_{OCT}$ spinel transition with

75 increasing pressure (8-15 GPa at room temperature) [15,16]. However, K-edge x-ray magnetic circular

76 dichroism and x-ray emission spectroscopy measurements are interpreted as an Fe^{2+} transition on the

77 octahedral site from high- to intermediate-spin at 12-16 GPa [7]. An additional hypothesis, based on X-ray

78 diffraction measurements, is that Fe_3O_4 has a phase transition from magnetite ($Fd\bar{3}m$ symmetry,

79 $\left[Fe^{3+}\right]_{TET}\left[Fe^{2+/3+}Fe^{2+/3+}\right]_{OCT}$, inverse spinel) to a new high-pressure phase, h-Fe_3O_4 (*Pbcm* symmetry,

80 $\left[Fe^{2+}\right]_{TET}\left[Fe^{3+}Fe^{3+}\right]_{OCT}$, normal spinel) between 10-20 GPa (300 K) [17-19]. The h-Fe_3O_4 crystal structure

81 is a $CaMn_2O_4$-type structure[18] (Fig. 1). No studies have yet been done on the spin-state of Fe in h-Fe_3O_4.

82 More recent X-ray diffraction measurements and Mössbauer spectroscopy experiments [4] as well as x-ray

83 absorption spectroscopy and Fe K-edge x-ray magnetic circular dichroism measurements [20] find magnetite

84 remains inverse spinel up to 25 GPa. Above 15 GPa, the measurements suggest the Fe electrons

85 delocalize [4], exhibiting a continuous decrease in moment [20] rather than undergoing a spin transition.

86 The measurements just discussed suggest four possible and quite different transitions with

87 pressure: charge reordering in magnetite (inverse to normal spinel), spin transition in magnetite (high- to

88 intermediate spin), electron delocalization in magnetite, or a structural transition to a new phase

89 (magnetite to h-Fe_3O_4). The goal of this paper is to calculate, using quantum-mechanical *ab initio*

90 methods, the spin state of Fe as a function of pressure in Fe_3O_4 magnetite and h-Fe_3O_4. Because spin is

91 linked to valence and site occupancy (and possibly magnetic ordering), multiple combinations of spin and

92 ordering in both magnetite and h-Fe_3O_4 need to be explored. This work will both help elucidate the

93 proposed pressure transitions that are actually occurring and the possibility of intermediate spin Fe in

94   magnetite. Section II describes the computational methods, including the *ab initio* details and the different

95   magnetic and spin states considered. Section III gives the results for magnetic and spin state behavior of

96   each structure of interest, including inverse spinel (section III A), normal spinel (section III B), and h-

97   Fe_3O_4 (section III C). The implications of these results for the stable phase as a function of pressure are

98   given in section III D and section III D provides useful elastic constant data.

99

100

101

II. METHODS

In this study we used density functional theory (DFT) methods as implemented in the Vienna Ab Initio Simulation Package (VASP) [21]. VASP calculations were performed with the projector-augmented wave method (electronic configuration: $2s^2\ 2p^4$ for oxygen, $3p^6\ 3d^7\ 4s^1$ for Fe) [22] using the Generalized Gradient Approximation (GGA) exchange-correlation with the Perdew-Burke-Ernzerhof (PBE) parameterization [23] and a cutoff energy for the planewave basis functions of 600 eV. A $2 \times 2 \times 2$ Monkhorst-Pack k-point mesh was used for sampling the Brillouin zone of the reciprocal space for all structures. All k-point meshes and energy cutoffs were chosen to have a convergence of less than 0.005 eV in energies and 0.02 Å^3/atom in volume. A Hubbard U parameter [10] was applied to provide more accurate electronic structure for the localized d-orbitals, and is necessary to stabilize distinct Fe^{2+} and Fe^{3+} atoms [24]. The invariant spin-polarized GGA+U scheme is used [25] and U is added to Fe atoms only. We used U, the on-site Coulomb interaction parameter, equal to 4.6 eV and J, the effective on-site exchange interaction parameter, equal to 0.544 eV, consistent with previous work on Fe_3O_4 [24].

All calculations were performed as spin polarized. Individual moments were allowed to relax and the total net moment of the cell was fixed. The spin and magnetic arrangements were created by setting initial magnetic moments on each atom and fixing the total net moment of the cell. Spins on the individual atoms were allowed to fully relax in the calculations. In some cases, a desired spin state with a given fixed total moment may relax to another spin state with the same total net moment. Details on fixed total net moments, initial moments, and final relaxed moments are given below.

A. Computational structural details

A central goal of this study is to calculate the spin state of Fe as a function of pressure in magnetite. The structure of magnetite may change with pressure and therefore three structures will be considered in the calculations in order to map the entire pressure space: inverse-spinel magnetite, normal-spinel magnetite, and h-Fe_3O_4 (Table I).

In the remainder of the paper, the following notation will be used:

127
$$\left[(-)Fe_{SPIN}^{valence}(-)Fe_{SPIN}^{valence}\right]_{TET}\left[(-)Fe_{SPIN}^{valence}(-)Fe_{SPIN}^{valence}(-)Fe_{SPIN}^{valence}(-)Fe_{SPIN}^{valence}\right]_{OCT}$$

128   [ ]$_{TET/OCT}$ denotes the spin, valence, and magnetic ordering for the tetrahedral (TET)/octahedral (OCT) sites

129   (Fig. 1). A "−" in front of Fe denotes that the spin points in the opposite direction from Fe without a "−".

130   Only collinear spins are considered. The superscript/subscript after the Fe marks the valence/spin of that

131   Fe atom. Spin will be represented by HS (high-spin), IS (intermediate-spin), and LS (low-spin) and the

132   magnetic moment for each spin and valence state is given in Table II. The six Fe atoms represent the six

133   Fe atoms in the fourteen atom primitive unit cell of Fe_3O_4[17].

134
135   **Table I:** Three structures are explored in the calculations. Magnetite may undergo an inverse to normal
136   spinel transition with pressure. Magnetite may also undergo a phase transition to h-Fe_3O_4 with pressure.
137   The spin state of Fe within all three structures is necessary to gain a complete understanding of the high-
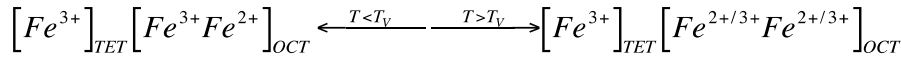138   pressure spin states.
139

Low-pressure	High-pressure	
magnetite, inverse spinel	magnetite, normal spinel	h-Fe_3O_4, normal spinel
$\left[Fe^{3+}\right]_{TET}\left[Fe^{2+}Fe^{3+}\right]_{OCT}$	$\left[Fe^{2+}\right]_{TET}\left[Fe^{3+}Fe^{3+}\right]_{OCT}$ OR	$\left[Fe^{2+}\right]_{TET}\left[Fe^{3+}Fe^{3+}\right]_{OCT}$
Imma symmetry	$Fd\bar{3}m$ symmetry	*Pbcm* symmetry
Random distribution of Fe^{2+} and Fe^{3+} on the *OCT* site.		High-pressure phase.
Fig. 1(a)	Fig. 1(a)	Fig. 1(b)

140
141
142   **Table II:** Total number of unpaired electrons and magnetic moment (μ_B) for each spin state and valence
143   state (Fe^{2+} and Fe^{3+}).
144

valence	HS high-spin	IS intermediate-spin	LS low-spin
Fe^{2+}	4	2	0
Fe^{3+}	5	3	1

145

146

147   *1. Magnetite at ambient conditions: inverse spinel*

148   Fe occupies both tetrahedral (*TET*) and octahedral (*OCT*) sites in magnetite (Fig. 1) at ambient

149   conditions. The magnetism in magnetite is due to the ferrimagnetic ordering of Fe spins between the *TET*

150   and *OCT* sites (Fig. 1). The known phases for the magnetite at lower pressure include both a low-

151   temperature monoclinic phase with ordered Fe^{2+} and Fe^{3+} and a disordered *Fd-3m* symmetry structure. At

152   120 K (T_V) magnetite undergoes an electronic transition, the Verwey transition, which corresponds to a

153   change in electrical conductivity [14] due to the transition:

154           $$\left[Fe^{3+}\right]_{TET}\left[Fe^{3+}Fe^{2+}\right]_{OCT} \xleftarrow{T<T_V} \xrightarrow{T>T_V} \left[Fe^{3+}\right]_{TET}\left[Fe^{2+/3+}Fe^{2+/3+}\right]_{OCT}$$

155   When $T > T_V$, there is a statistical distribution of Fe^{2+} and Fe^{3+} with an average charge of $Fe^{2.5+}$ on the

156   octahedral sites leading to high electrical conductivity. For $T < T_V$, Fe^{2+} and Fe^{3+} become ordered on the

157   *OCT* site and, as a consequence, conductivity is lost [14]. Charge ordering has been confirmed by resonant x-

158   ray diffraction experiments [26,27]. DFT calculations are technically at absolute zero, since the energy

159   solution corresponds to the ground state energy.

160   The focus of this study is on pressure-induced spin transitions in magnetite at room temperature

161   for direct comparison with the experimental spin-transition study by Ding et al. [7]. Ideally, both phases

162   would be included for a complete study of the spin state with and without the effect of charge-ordering.

163   Instead, a single phase, the charge-ordered structure $\left[Fe^{3+}\right]_{TET}\left[Fe^{3+}Fe^{2+}\right]_{OCT}$, was used as an

164   approximation of the true statistical distribution. This is a necessary approximation to make the

165   calculations practical and an acceptable approximation given the goal of the work to study the spin

166   transition. Representing the random distribution of Fe^{2+} and Fe^{3+} atoms in the $T > T_V$ charge-disordered

167   structure $\left[Fe^{3+}\right]_{TET}\left[Fe^{2+/3+}Fe^{2+/3+}\right]_{OCT}$ would require a large cell that is computationally impractical for

168   this work. Furthermore, the pressure-dependence of T_V is not yet clear and at the higher pressures of the

169   mantle the charge-ordered structure may in fact be the most stable structure at temperatures of interest.

170   In terms of the accuracy of the approximation, both the monoclinic (charge-ordered) and *Fd-3m*

171   (charge-averaged) structures are clearly quite similar in energy, as the Verwey transition occurs at

172   T_{Verwey}=120K. This generally argues for charge ordering being a small contribution to the energy, on the

173   order of just $kT_{Verwey}\sim 10$ meV/Fe atom. The results of this study will show the energy scale of the high-

174   to intermediate- spin transition in magnetite is 1.01 eV/f.u. (~ 340 meV/Fe). Therefore, the energy change

175   due to charge ordering differences should not change the energetics of the spin transition enough to

176   stabilize intermediate-spin and in general would have negligible effects on the transitions of interest.

177   The charge-ordered inverse-spinel magnetite structure was created by starting with $Fd\bar{3}m$

178   symmetry and the experimental atomic positions (Fe(tet) 0.125 0.125 0.125, Fe(oct) 0.5 0.5 0.5, O

179   .2549 .2549 .2549, a=b=c=8.3965, $\alpha=\beta=\gamma=90°$)[17,28]. To allow for ordering of Fe^{2+} and Fe^{3+}, a 14-atom unit

180   cell was created[29] and the symmetry on the OCT site was reduced to *Imma* by making the 4th and 5th Fe

181   atoms Fe^{2+}, consistent with Wenzel and Steinle-Neumann (2007). The choice of the *Imma* charge-ordered

182   inverse-spinel magnetite structure is a practical approximation that has allowed us to elucidate the

183   magnetite spin behavior with minimal loss of accuracy.

2. Magnetite at high pressure: normal spinel

185   Magnetite may undergo an inverse to normal spinel transition near 8 GPa [15,16]. 8 GPa is near the

186   possible spin-transition region, therefore spin transitions should also be considered in normal spinel. The

187   normal-spinel structure was created from the experimentally identified atom positions for this structure in

188   a 14-atom unit cell with $Fd\bar{3}m$ symmetry [17]. In the input file all TET atoms were specified as Fe^{2+} and all

189   OCT atoms were specified as Fe^{3+} by setting their respective initial magnetic moments.

3. Phase change in magnetite at high-pressure: h-Fe₃O₄

191   The high-pressure magnetite phase, h-Fe_3O_4 has a CaMn₂O₄-type structure with *Pbcm* space

192   group [18], with the magnetic ordering of Fe^{2+} on the tetrahedral site and Fe^{3+} on the octahedral site

193     $\left[Fe^{2+}\right]_{TET}\left[Fe^{3+}Fe^{3+}\right]_{OCT}$ (Fig. 1b). Within the calculations, the *Pbcm* symmetry relaxes to CaTi₂O₄ -type

194   *Bbmm*[29], consistent with [19] and [17]. A 28-atom unit cell was used.

195   A. Calculations under pressure

196   High-pressure behavior of magnetite (inverse spinel and normal spinel) and h-Fe_3O_4 was studied

197   by performing fixed volume calculations. The ions were allowed to relax but cell shape and volume were

198   fixed – this corresponds to ISIF=2 in the VASP INCAR file[29]. In the magnetite 14-atom unit cell, the

199   volume space grid was 155, 150, 145, 140, 135, 130, 125, and 120 $Å^3$. In the 28-atom h-Fe_3O_4 unit cell

200   the volume space grid was 290, 285, 280, 275, 270, 265, 260, 250, 240, 230 and 220 $Å^3$. For each

201   structure and spin state, energy as a function of volume, E(V), was fit to a 3rd-order Birch-Murnaghan

202   equation of state to determine the energy and volume as a function of pressure. From E(P) and V(P),

203   enthalpy as a function of pressure, H(P)=E(P)+P·V(P), and the equation of state parameters were found.

204

205   B. Calculating the spin state

206   Our goal is to understand the spin state of Fe in Fe_3O_4. Since the spin state of Fe could be linked

207   to site coordination (TET vs. OCT), magnetic ordering, charge ordering, and charge coordination (valence),

208   all these factors must be studied in order to have a full understanding of the spin state of Fe in Fe_3O_4. In

209   this section, the spin calculations are laid out in detail.

210   To motivate the spin states studied, we first consider the spin related changes measured as a

211   function of pressure by Ding et al., 2008. Their *K*-edge x-ray magnetic circular dichroism measurements

212   show a drop in total magnetic moment by half (a decrease of $4\mu_B$ to $2\mu_B$ /formula unit, which would be

213    $8\mu_B$ to $4\mu_B$ in our fourteen-atom computational unit cell) and their X-ray emission-spectroscopy

214   measurements find a drop of peak intensity by ~ 15%, meaning ~15% of unpaired electrons have reduced

215   their spins. In the formula unit of inverse-spinel magnetite (3 Fe atoms) $\left[-Fe^{3+}\right]_{TET}\left[Fe^{3+}Fe^{2+}\right]_{OCT}$, there

216   are two Fe^{3+} atoms (five unpaired electrons each, Table II) and one Fe^{2+} atom (four unpaired electrons,

217   Table II), with a total of fourteen unpaired electrons. If Fe^{2+} goes from HS to IS (drop from four to two

218   unpaired electrons), the reduction in unpaired electrons is 14%, consistent with measurements [7]. Another

219   spin transition that would be consistent with measurements but not considered by Ding et al. (2008), is

220   one Fe^{3+} atom (either on the TET or OCT site, but not both) going through a HS to IS transition,

221   corresponding to a drop in unpaired electrons by 2 (14%). Therefore both intermediate-spin Fe^{2+} and Fe^{3+}

222   are considered in this study. Even though transitions from HS to LS Fe^{2+} or Fe^{3+} are too high of a drop in

223   unpaired electrons to match the experimental measurements of Ding, et al., these larger spin state changes

224   are also considered in order to map out the entire spin space.

225

226   *1. Calculating the spin state of inverse spinel*

227   All calculations started with *Imma* symmetry (see section II A), which allowed for ordering of

228   Fe^{2+} and Fe^{3+} on the OCT sites. In VASP, the initial magnetic moments and moment directions on each Fe

229   atom can be specified but only the total net magnetic moment (NMM) in the 14-atom unit cell can be

230   fixed throughout the calculation. Therefore the direction of the moments on individual atoms can relax to

231   different orderings as long as the NMM remains fixed. For inverse spinel,

232    $\left[-Fe_{HS}^{3+}-Fe_{HS}^{3+}\right]_{TET}\left[Fe_{HS}^{3+}Fe_{HS}^{2+}Fe_{HS}^{2+}Fe_{HS}^{3+}\right]_{OCT}$, the net moment is 8 μ_B because the individual magnetic

233   moments (in μ_B) are - 5 - 5 + 5 + 4 + 4 + 5, which sum to 8 (see Table II, Table III, Table IV).

234   The magnetic ordering schemes considered for HS are given in Table III. These are all possible

235   distinct (i.e., symmetrically inequivalent) magnetic orderings in the 14-atom unit cell. Besides the

236   ferromagnetic arrangement, all magnetic orderings are ferrimagnetic except one with a net moment of 0,

237   which is antiferromagnetic.

238   **Table III**: All possible magnetic arrangements in 14-atom inverse-spinel magnetite cell. If the arrangement/spin is
239   metastable, then the initial moments specified in calculation are *locally* meta-stable after the final relaxations.
240   Otherwise the initial moments are *not locally* meta-stable and relaxed to different individual moments with the same
241   total net moment. Italicized abbreviations in the left column match those in Fig. 2.

	TET		OCT					
	Fe1	Fe2	Fe3	Fe4	Fe5	Fe6	Net Moment	Locally meta-stable

Magnetic orderings, all high-spin

	TET		OCT					
Ferrimagnetic (*mag1*) $\left[-Fe_{HS}^{3+}-Fe_{HS}^{3+}\right]_{TET}\left[Fe_{HS}^{3+}Fe_{HS}^{2+}Fe_{HS}^{2+}Fe_{HS}^{3+}\right]_{OCT}$	-5	-5	5	4	4	5	8	Yes

Configuration								
Antiferromagnetic (*NMM0*) $\left[-Fe_{HS}^{3+}Fe_{HS}^{3+}\right]_{TET}\left[-Fe_{HS}^{3+}Fe_{HS}^{2+}-Fe_{HS}^{2+}Fe_{HS}^{3+}\right]_{OCT}$	-5	5	-5	4	-4	5	0	Yes
Ferrimagnetic (*NMM2*) $\left[Fe_{HS}^{3+}Fe_{HS}^{3+}\right]_{TET}\left[Fe_{HS}^{3+}-Fe_{HS}^{2+}-Fe_{HS}^{2+}Fe_{HS}^{3+}\right]_{OCT}$	5	5	5	-4	-4	5	2	Yes
Ferrimagnetic (*NMM2**) $\left[Fe_{HS}^{3+}Fe_{HS}^{3+}\right]_{TET}\left[-Fe_{HS}^{3+}-Fe_{HS}^{2+}-Fe_{HS}^{2+}Fe_{HS}^{3+}\right]_{OCT}$	5	5	-5	-4	-4	5	2	Yes
Ferrimagnetic (*NMM8*) $\left[Fe_{HS}^{3+}Fe_{HS}^{3+}\right]_{TET}\left[-Fe_{HS}^{3+}Fe_{HS}^{2+}Fe_{HS}^{2+}-Fe_{HS}^{3+}\right]_{OCT}$	5	5	-5	4	4	-5	8	Yes
Ferrimagnetic (*NMM12*) $\left[Fe_{HS}^{3+}Fe_{HS}^{3+}\right]_{TET}\left[Fe_{HS}^{3+}-Fe_{HS}^{2+}-Fe_{HS}^{2+}Fe_{HS}^{3+}\right]_{OCT}$	5	5	5	-4	-4	5	12	Yes
Ferrimagnetic (*NMM18*) $\left[-Fe_{HS}^{3+}Fe_{HS}^{3+}\right]_{TET}\left[Fe_{HS}^{3+}Fe_{HS}^{2+}Fe_{HS}^{2+}Fe_{HS}^{3+}\right]_{OCT}$	-5	5	5	4	4	5	18	Yes
Ferromagnetic (*NMM28*) $\left[Fe_{HS}^{3+}Fe_{HS}^{3+}\right]_{TET}\left[Fe_{HS}^{3+}Fe_{HS}^{2+}Fe_{HS}^{2+}Fe_{HS}^{3+}\right]_{OCT}$	5	5	5	4	4	5	28	Yes

242
243   Energies for all these magnetic orderings as a function of pressure have been calculated and are

244   discussed in section 3.1. The most stable magnetic ordering

245     $\left[-Fe_{HS}^{3+}-Fe_{HS}^{3+}\right]_{TET}\left[Fe_{HS}^{3+}Fe_{HS}^{2+}Fe_{HS}^{2+}Fe_{HS}^{3+}\right]_{OCT}$ was used as the starting configuration for all spin-

246   transition calculations. The atomic positions and individual moments were then allowed to relax. There

247   are two measures of spin stability. The first measure is that individual moments for a fixed NMM must

248   retain their starting spin state after relaxation. If the spin state on the individual Fe atoms relaxes to

249   different moments for a given initial NMM, the initial spin arrangement is not stable. If the individual

250   spin states are the same after relaxation, then the spin state is considered *locally* stable. For each locally

251   stable spin state we explore a second measure to determine if the spin state is stable *globally*. Global

252   stability is determined by plotting the enthalpy curves for different spin states as a function of pressure

253   and determining the most stable spin state of all the spin arrangements considered at each pressure.

254   In the 14-atom computational cell (six Fe atoms) HS inverse-spinel magnetite has a net moment

255   of 8. Calculations with all intermediate-spin (net moment 4) were not locally stable; the cell relaxed to

256   high-spin Fe^{3+} on the *TET* and *OCT* sites and intermediate-spin Fe^{2+} on the *OCT* (net moment of 4).

257   Calculations with all low-spin (net moment 0) were also not locally stable. The calculation relaxed to

258   high-spin Fe^{3+} on the *TET* and OCT and low-spin Fe^{2+} on the OCT (net moment of 0). Decreasing the

259   moment of Fe^{3+} on *TET* without reducing the moment on the OCT increases the total net moment (12 for IS

260   Fe^{3+}, 16 for LS Fe^{3+}) and is not locally stable. IS Fe^{3+} on *TET* relaxed to all high-spin normal spinel, or

261    $\left[-Fe^{2+}_{HS} - Fe^{2+}_{HS}\right]_{TET}\left[Fe^{3+}_{HS}Fe^{3+}_{HS}Fe^{3+}_{HS}Fe^{3+}_{HS}\right]_{OCT}$. LS Fe^{3+} on TET relaxed to normal spinel with IS Fe^{2+} on

262   the TET site, or $\left[-Fe^{2+}_{IS} - Fe^{2+}_{IS}\right]_{TET}\left[Fe^{3+}_{HS}Fe^{3+}_{HS}Fe^{3+}_{HS}Fe^{3+}_{HS}\right]_{OCT}$.

263   Unlike spin transitions on the *TET* site, decreasing the moment of Fe^{2+} or Fe^{3+} on the OCT site

264   decreases the total net moment (4 for IS Fe^{2+} and Fe^{3+}, 0 for LS Fe^{2+} and Fe^{3+}). Magnetite with

265   intermediate-spin Fe^{3+} on the OCT site has the same total net magnetic moment as magnetite with Fe^{2+} on

266   the OCT site. During relaxation, intermediate-spin Fe^{3+} was only locally stable in the calculation for very

267   low-pressures and never globally more stable than high-spin. For higher pressures, Fe^{3+} on the OCT site

268   changed to high-spin and Fe^{2+} relaxed to intermediate-spin. For a total net moment of 4, it is more

269   energetically favorable for Fe^{2+} to change from high- to intermediate-spin than for Fe^{3+}. Likewise, low-

270   spin Fe^{3+} was not stable in the calculation. For a fixed total moment of 0, the calculations relaxed to LS

271   Fe^{2+} instead of Fe^{3+}, suggesting Fe^{3+} in inverse-spinel magnetite is only stable as high-spin.

272

273

274   *2. Calculating the spin state of normal spinel*

275   Since there may be an inverse to normal spinel transition in magnetite, spin transition calculations

276   were also conducted in the normal spinel structure as a function of pressure (Fig. 3). All possible spin

277   states (HS, IS, LS) on the *TET* and OCT sites were explored (Table V). Spin transitions were considered on

278   both *TET* and OCT sites as well as individually on the *TET* or OCT site (Table V).

279   A number of the normal-spinel spin configuration calculations were not locally stable.

280   Calculations of all intermediate-spin Fe relaxed to inverse-spinel HS. Calculations of all low-spin Fe

281   relaxed to Fe with moments slightly reduced from HS, maintaining a net moment of 4. Reducing the spin

282   of Fe^{3+} to LS or IS on the OCT site was not energetically favorable. To maintain the net magnetic moment,

13

283   the system preferred to change the *TET* site to HS Fe^{3+} (inverse spinel), and reduce the total moment on

284   every Fe atom on the *OCT* site.

285   *3. Calculating the spin state of h-Fe₃O₄*

286

287   The correct magnetic ordering also needs to be determined in the high-pressure phase, h-Fe_3O_4.

288   The experimentally determined h-Fe_3O_4 unit cell is twice that of magnetite, therefore spins and magnetic

289   ordering are given for the 12 Fe atoms in the unit cell (out of 28 total atoms). Only magnetic orderings

290   that fit within the crystallographic unit cell are considered (Table VI). Trying every possible magnetic

291   arrangement in the 28-atom cell would be computationally impractical. Therefore, only a few

292   representative magnetic orderings were chosen based on the results in magnetite (Fig. 2): the same

293   magnetic ordering as magnetite, magnetic ordering yielding a net magnetic moment of 0, and

294   ferromagnetic. Energetics and details of the different magnetic arrangements for h-Fe_3O_4 are discussed in

295   section 3.3.

296   Calculations starting with all intermediate-spin or all low-spin Fe on the *OCT* and *TET* sites were

297   not locally stable and relaxed to a combination of high-, low-, and reduced-spin Fe^{2+} and Fe^{3+} with a net

298   moment of 16 (8 for all low-spin). Calculations that started with intermediate-spin Fe^{3+} on the *OCT* site

299   were not locally stable and relaxed to a combination of high- and low-spin Fe atoms and the *TET* site

300   became Fe^{2+}.

301

III. RESULTS

302

303

304   This section is organized as follows. First, magnetic ordering and spin transitions within inverse-

305   spinel magnetite are presented (section A). Then results on magnetic ordering and spin transitions in

306   normal-spinel magnetite are given (section B). The stable magnetic arrangements and spin states in h-

307   Fe_3O_4 are presented in section C. Section D discusses the impact of magnetic order, spin and

308   normal/inverse spinel on the pressure-induced phase transition of inverse-spinel magnetite to h-Fe_3O_4.

309   Finally, section E gives the equations of state of the key phases as a function of pressure.

310

A. Magnetic ordering and spin transitions in inverse-spinel magnetite

312

313   The strong magnetic moment in inverse-spinel magnetite occurs due to ferrimagnetic

314     $\left[-Fe_{HS}^{3+}-Fe_{HS}^{3+}\right]_{TET}\left[Fe_{HS}^{3+}Fe_{HS}^{2+}Fe_{HS}^{2+}Fe_{HS}^{3+}\right]_{OCT}$ ordering between the TET and OCT sites [14]. We test that this

315   is the correct magnetic ordering in inverse-spinel magnetite by comparing the enthalpies as a function of

316   pressure for multiple magnetic arrangements in the charge-ordered structure. The relative enthalpies of

317   the different magnetic orderings are plotted in Fig. 2(a). The figure clearly shows that ferrimagnetic

318   ordering between the TET and OCT sites $\left[-Fe_{HS}^{3+}-Fe_{HS}^{3+}\right]_{TET}\left[Fe_{HS}^{3+}Fe_{HS}^{2+}Fe_{HS}^{2+}Fe_{HS}^{3+}\right]_{OCT}$ (*mag1*) is the most

319   stable for all pressures by more than 140 meV/f.u. and is used for the remainder of the inverse-spinel

320   magnetite spin studies. There is no magnetic ordering transition under pressure in magnetite.

321   Ferromagnetic ordering (FM) is over 0.8 eV/f.u. less stable than ferromagnetic *mag1*.

322   The spin transition pressure of Fe is considered on both TET and OCT sites (Fig. 2(b)). Table IV

323   lists the spin states considered, the initial individual moments specified on each atom, and the total

324   magnetic moment. Fe^{3+} on the TET site in inverse-spinel magnetite remains HS for all pressures. Neither

325   all intermediate- nor low-spin Fe on the TET site are locally stable in the calculations (Table IV).

326   The relative enthalpies of high-, intermediate-, and low-spin Fe^{2+} on the OCT site are plotted in

327   Fig. 2(b). Intermediate-spin Fe^{2+} is 1 eV/f.u. less stable at ambient pressure than high-spin Fe. Low-spin

328 Fe^{2+} is 1.2 eV/f.u. less stable than high-spin. For all pressures up to 45 GPa (the highest considered), Fe^{2+}

329 and Fe^{3+} in inverse-spinel magnetite will remain high-spin. To be sure that the instability of the

330 intermediate-spin state was not due to our specific value of U, a range of U values were explored.

331 Increasing U stabilizes high-spin magnetite with respect to intermediate-spin and decreases the h-Fe_3O_4 to

332 magnetite phase transition pressure[29].

333   The experimentally observed phases involve unit cells significantly larger than 14-atom unit cell.

334 Pursuing larger cells with more complex charge ordering would greatly complicate and slow the

335 calculations. In fact, in addition to the 14-atom charge-ordered structure with *Imma* symmetry, the 56-

336 atom structure charge-ordered structure with *P2/c* monoclinic symmetry (*Pmca* pseudosymmetry) [27] was

337 also used. The larger unit cell was calculated with intermediate-spin Fe^{2+} on the octahedral site.

338 Intermediate spin was not metastable in the calculations; the Fe spins relaxed to a mixture of high- and

339 low-spin Fe^{2+} and Fe^{3+}. In VASP, only the total moment can be fixed; moments on individual atoms

340 cannot be fixed. The larger unit cell made controlling the individual spins on the Fe atoms

341 computationally impossible; therefore the simpler *Imma* symmetry was chosen for easier control of Fe's

342 spin state.

343

344 **Table IV:** Summary of all inverse-spinel magnetite spin states considered in this study, organized by site.
345 Initial moments for each spin state and total fixed net moment for cell in the 14-atom cell. Italicized
346 abbreviations in the left column match those in Fig. 2(b). When a calculation is not *locally* meta-stable,
347 the final spin state after relaxation is noted and explained in the text.
348

	TET		OCT					
	Fe1	Fe2	Fe3	Fe4	Fe5	Fe6	Net Moment	Locally meta-stable

Spin-transitions on both sites

	Fe1	Fe2	Fe3	Fe4	Fe5	Fe6	Net Moment	Locally meta-stable
All high-spin (*mag1*) $\left[-Fe_{HS}^{3+}-Fe_{HS}^{3+}\right]_{TET}\left[Fe_{HS}^{3+}Fe_{HS}^{2+}Fe_{HS}^{2+}Fe_{HS}^{3+}\right]_{OCT}$	-5	-5	5	4	4	5	8	yes
All intermediate-spin $\left[-Fe_{IS}^{3+}-Fe_{IS}^{3+}\right]_{TET}\left[Fe_{IS}^{3+}Fe_{IS}^{2+}Fe_{IS}^{2+}Fe_{IS}^{3+}\right]_{OCT}$	-3	-3	3	2	2	3	4	no ➜ *IS 2+ OCT*
All low-spin $\left[-Fe_{LS}^{3+}-Fe_{LS}^{3+}\right]_{TET}\left[Fe_{LS}^{3+}Fe_{LS}^{2+}Fe_{LS}^{2+}Fe_{LS}^{3+}\right]_{OCT}$	-1	-1	1	0	0	1	0	no ➜ *LS 2+ OCT*

Tetrahedral (TET) site spin-transitions

Intermediate-spin Fe^{3+} $\left[-Fe^{3+}_{IS}-Fe^{3+}_{IS}\right]_{TET}\left[Fe^{3+}_{HS}Fe^{2+}_{HS}Fe^{2+}_{HS}Fe^{3+}_{HS}\right]_{OCT}$	-3	-3	5	4	4	5	12	no ➔normal spinel *HS TET, OCT*
Low-spin Fe^{3+} $\left[-Fe^{3+}_{LS}-Fe^{3+}_{LS}\right]_{TET}\left[Fe^{3+}_{HS}Fe^{2+}_{HS}Fe^{2+}_{HS}Fe^{3+}_{HS}\right]_{OCT}$	-1	-1	5	4	4	5	16	no ➔normal spinel *IS 2+ TET*

Octahedral (OCT) site spin-transitions

Intermediate-spin Fe^{2+} (*IS 2+ OCT*) $\left[-Fe^{3+}_{HS}-Fe^{3+}_{HS}\right]_{TET}\left[Fe^{3+}_{HS}Fe^{2+}_{IS}Fe^{2+}_{IS}Fe^{3+}_{HS}\right]_{OCT}$	-5	-5	5	2	2	5	4	yes
Intermediate-spin Fe^{3+} $\left[-Fe^{3+}_{HS}-Fe^{3+}_{HS}\right]_{TET}\left[Fe^{3+}_{IS}Fe^{2+}_{HS}Fe^{2+}_{HS}Fe^{3+}_{IS}\right]_{OCT}$	-5	-5	3	4	4	3	4	Low pressure only ➔ *IS 2+ OCT*
Low-spin Fe^{2+} (*LS 2+ OCT*) $\left[-Fe^{3+}_{HS}-Fe^{3+}_{HS}\right]_{TET}\left[Fe^{3+}_{HS}Fe^{2+}_{LS}Fe^{2+}_{LS}Fe^{3+}_{HS}\right]_{OCT}$	-5	-5	5	0	0	5	0	yes
Low-spin Fe^{3+} $\left[-Fe^{3+}_{HS}-Fe^{3+}_{HS}\right]_{TET}\left[Fe^{3+}_{LS}Fe^{2+}_{HS}Fe^{2+}_{HS}Fe^{3+}_{LS}\right]_{OCT}$	-5	-5	1	4	4	1	0	no ➔ *LS 2+ OCT*

349

350

351   B. Magnetic ordering and spin transitions in normal-spinel magnetite

352

353   Normal spinel is less stable than inverse spinel (mag1) by over 0.77 eV/f.u. for all pressures (Fig.

354 3). As in the case of inverse spinel, intermediate- and low-spin Fe^{2+} on the *TET* site in normal spinel are

355 energetically unfavorable with respect to high-spin iron. Spin transitions on the *OCT* site were considered

356 (Table V), especially intermediate-spin Fe^{3+}, which has a net moment of four. However, changing to

357 intermediate-spin on the *OCT* site was not locally stable and upon relaxation the system formed inverse

358 spinel (Fe^{3+} on the *TET* site) and reduced the moment of Fe^{2+} on the *OCT* site (without actually flipping an

359 electron spin to fully form the intermediate-spin state).

360 **Table V**: Spin states considered in the fourteen-atom normal-spinel magnetite unit cell. Italicized
361 abbreviations in the left column match those in Fig. 3. When a given spin or magnetic arrangement is not
362 locally meta-stable, the final spin state after relaxation is noted and explained in the text.

363

364

	TET		OCT					
	Fe1	Fe2	Fe3	Fe4	Fe5	Fe6	Net moment	Locally meta-stable
Spin-transitions on both sites								
All high-spin (*HS TET, OCT*) $\left[-Fe_{HS}^{2+}-Fe_{HS}^{2+}\right]_{TET}\left[Fe_{HS}^{3+}Fe_{HS}^{3+}Fe_{HS}^{3+}Fe_{HS}^{3+}\right]_{OCT}$	-4	-4	5	5	5	5	12	Yes
All intermediate-spin $\left[-Fe_{IS}^{2+}-Fe_{IS}^{2+}\right]_{TET}\left[Fe_{IS}^{3+}Fe_{IS}^{3+}Fe_{IS}^{3+}Fe_{IS}^{3+}\right]_{OCT}$	-2	-2	3	3	3	3	8	no ➜ *mag1*
All low-spin $\left[-Fe_{LS}^{2+}-Fe_{LS}^{2+}\right]_{TET}\left[Fe_{LS}^{3+}Fe_{LS}^{3+}Fe_{LS}^{3+}Fe_{LS}^{3+}\right]_{OCT}$	0	0	1	1	1	1	4	no ➜ reduced moments
Tetrahedral (TET) site spin-transitions								
Intermediate-spin Fe^{2+} (*IS 2+ TET*)	-2	-2	5	5	5	5	16	Yes
Low-spin Fe^{2+} (*LS 2+ TET*) $\left[-Fe_{LS}^{2+}-Fe_{LS}^{2+}\right]_{TET}\left[Fe_{HS}^{3+}Fe_{HS}^{3+}Fe_{HS}^{3+}Fe_{HS}^{3+}\right]_{OCT}$	0	0	5	5	5	5	20	Yes
Octahedral (OCT) site spin-transitions								
Intermediate-spin Fe^{3+} $\left[-Fe_{HS}^{2+}-Fe_{HS}^{2+}\right]_{TET}\left[Fe_{IS}^{3+}Fe_{IS}^{3+}Fe_{IS}^{3+}Fe_{IS}^{3+}\right]_{OCT}$	-4	-4	3	3	3	3	4	no ➜ inverse spinel with reduced moments on OCT
Low-spin Fe^{3+} $\left[-Fe_{HS}^{2+}-Fe_{HS}^{2+}\right]_{TET}\left[Fe_{LS}^{3+}Fe_{LS}^{3+}Fe_{LS}^{3+}Fe_{LS}^{3+}\right]_{OCT}$	-4	-4	1	1	1	1	-4	no ➜ inverse spinel with reduced moments on OCT

365

366   C. Magnetic ordering and spin transitions in h-Fe$_3$O$_4$

367

368   The most stable magnetic ordering in h-Fe$_3$O$_4$ is antiferromagnetic ordering (h-NMM0) with a

369   total net moment of 0 (Fig. 4(a)). Ferrimagnetic ordering between *TET* and *OCT* (h-NMM24) with a net

370   moment of 24 has very similar energetics to the antiferromagnetic ordering, differing by ~ 20 meV/f.u..

371   There is an approximately 140 meV/f.u. difference between ferrimagnetic and ferromagnetic ordering in

372   h-Fe$_3$O$_4$.

373   Intermediate-spin Fe^{2+} on the *TET* site is more than 0.84 eV/f.u. less stable than HS (Fig. 4b).

374   Low-spin Fe^{2+} on the *TET* site is more than 1.26 eV/f.u. less stable than HS Fe^{2+}. Ferrimagnetic LS Fe^{3+} on

18

375   the OCT site and ferromagnetic Fe^{3+} on the *OCT* site have similar enthalpies (to within 140 meV/f.u.), but

376   both are more than 2.1 eV/f.u. less stable than HS h-Fe_3O_4. Therefore high-spin Fe remains stable in both

377   *TET* and *OCT* sites for all pressures considered in this study (up to 70 GPa).

378   It is worth noting that in both magnetite and h-Fe_3O_4, spin lowering in Fe^{2+} was more stable than

379   spin lowering in Fe^{3+}. If the initial moments were set such that Fe^{3+} had a lower moment, the relaxations

380   tended to favor flipping the spin on the Fe^{2+} rather than on the Fe^{3+}. This demonstrates a clear coupling of

381   valence and spin state, with Fe^{3+} favoring high-spin more than Fe^{2+} in the magnetite structure. This result

382   might be expected due to the half-filled d-shell providing additional stabilization in the Fe^{3+} HS state.

383

384 **Table VI**: Magnetic orderings and spin arrangements considered in 28-atom h-Fe_3O_4. Italicized
385 abbreviations in the left column match those in Fig. 4. To conserve space, individual moments are not
386 listed. When a calculation is not locally stable, the final spin state after relaxation is noted and explained
387 in the text.

	Net moment	Locally meta-stable
Magnetic ordering arrangements, all high-spin		
Inverse spinel, ferrimagnetic (*mag1*) $[-Fe^{3+}_{HS}-Fe^{3+}_{HS}-Fe^{3+}_{HS}-Fe^{3+}_{HS}]_{TET}[Fe^{3+}_{HS}Fe^{3+}_{HS}Fe^{2+}_{HS}Fe^{2+}_{HS}Fe^{2+}_{HS}Fe^{2+}_{HS}Fe^{3+}_{HS}Fe^{3+}_{HS}]_{OCT}$	16	Yes
h-Fe_3O_4, anti-ferromagnetic (*h-NMM0*) $[Fe^{2+}_{HS}-Fe^{2+}_{HS}Fe^{2+}_{HS}-Fe^{2+}_{HS}]_{TET}[Fe^{3+}_{HS}-Fe^{3+}_{HS}Fe^{3+}_{HS}-Fe^{3+}_{HS}Fe^{3+}_{HS}-Fe^{3+}_{HS}Fe^{3+}_{HS}-Fe^{3+}_{HS}]_{OCT}$	0	Yes
h-Fe_3O_4, ferrimagnetic (*h-NMM24*) $[-Fe^{2+}_{HS}-Fe^{2+}_{HS}-Fe^{2+}_{HS}-Fe^{2+}_{HS}]_{TET}[Fe^{3+}_{HS}Fe^{3+}_{HS}Fe^{3+}_{HS}Fe^{3+}_{HS}Fe^{3+}_{HS}Fe^{3+}_{HS}Fe^{3+}_{HS}Fe^{3+}_{HS}]_{OCT}$	24	Yes
h-Fe_3O_4, ferromagnetic (*h-FM*) $[Fe^{2+}_{HS}Fe^{2+}_{HS}Fe^{2+}_{HS}Fe^{2+}_{HS}]_{TET}[Fe^{3+}_{HS}Fe^{3+}_{HS}Fe^{3+}_{HS}Fe^{3+}_{HS}Fe^{3+}_{HS}Fe^{3+}_{HS}Fe^{3+}_{HS}Fe^{3+}_{HS}]_{OCT}$	56	Yes
Spin-transitions on both sites		
All intermediate-spin $[-Fe^{2+}_{IS}-Fe^{2+}_{IS}-Fe^{2+}_{IS}-Fe^{2+}_{IS}]_{TET}[Fe^{3+}_{IS}Fe^{3+}_{IS}Fe^{3+}_{IS}Fe^{3+}_{IS}Fe^{3+}_{IS}Fe^{3+}_{IS}Fe^{3+}_{IS}Fe^{3+}_{IS}]_{OCT}$	16	no ➔ reduced moments
All low-spin $[-Fe^{2+}_{LS}-Fe^{2+}_{LS}-Fe^{2+}_{LS}-Fe^{2+}_{LS}]_{TET}[Fe^{3+}_{LS}Fe^{3+}_{LS}Fe^{3+}_{LS}Fe^{3+}_{LS}Fe^{3+}_{LS}Fe^{3+}_{LS}Fe^{3+}_{LS}Fe^{3+}_{LS}]_{OCT}$	8	no ➔ reduced moments
Tetrahedral (TET) site spin-transitions		
Intermediate-spin Fe^{2+} (*IS 2+ TET*) $[-Fe^{2+}_{IS}-Fe^{2+}_{IS}-Fe^{2+}_{IS}-Fe^{2+}_{IS}]_{TET}[Fe^{3+}_{HS}Fe^{3+}_{HS}Fe^{3+}_{HS}Fe^{3+}_{HS}Fe^{3+}_{HS}Fe^{3+}_{HS}Fe^{3+}_{HS}Fe^{3+}_{HS}]_{OCT}$	32	Yes
Low-spin Fe^{2+} (*LS 2+ TET*) $[-Fe^{2+}_{LS}-Fe^{2+}_{LS}-Fe^{2+}_{LS}-Fe^{2+}_{LS}]_{TET}[Fe^{3+}_{HS}Fe^{3+}_{HS}Fe^{3+}_{HS}Fe^{3+}_{HS}Fe^{3+}_{HS}Fe^{3+}_{HS}Fe^{3+}_{HS}Fe^{3+}_{HS}]_{OCT}$	40	Yes
Octahedral (OCT) site spin-transitions		
Intermediate-spin Fe^{3+} $[-Fe^{2+}_{HS}-Fe^{2+}_{HS}-Fe^{2+}_{HS}-Fe^{2+}_{HS}]_{TET}[Fe^{3+}_{IS}Fe^{3+}_{IS}Fe^{3+}_{IS}Fe^{3+}_{IS}Fe^{3+}_{IS}Fe^{3+}_{IS}Fe^{3+}_{IS}Fe^{3+}_{IS}]_{OCT}$	8	no ➔ reduced moments
Low-spin Fe^{3+}, ferromagnetic (*LS 3+ OCT*) $[Fe^{2+}_{HS}Fe^{2+}_{HS}Fe^{2+}_{HS}Fe^{2+}_{HS}]_{TET}[Fe^{3+}_{LS}Fe^{3+}_{LS}Fe^{3+}_{LS}Fe^{3+}_{LS}Fe^{3+}_{LS}Fe^{3+}_{LS}Fe^{3+}_{LS}Fe^{3+}_{LS}]_{OCT}$	24	Yes
Low-spin Fe^{3+}, ferromagnetic (*LS 3+ OCT*) $[-Fe^{2+}_{HS}-Fe^{2+}_{HS}-Fe^{2+}_{HS}-Fe^{2+}_{HS}]_{TET}[Fe^{3+}_{LS}Fe^{3+}_{LS}Fe^{3+}_{LS}Fe^{3+}_{LS}Fe^{3+}_{LS}Fe^{3+}_{LS}Fe^{3+}_{LS}Fe^{3+}_{LS}]_{OCT}$	-8	Yes

388

389

390   D. Phase transitions under pressure: inverse-spinel magnetite to h-Fe_3O_4 structure.

391
392   Based on the most stable spin states vs. pressure for inverse-spinel magnetite, normal-spinel

393   magnetite, and h-Fe_3O_4 there is a predicted phase transition from the inverse-spinel magnetite to h-Fe_3O_4

394   at 10 GPa. Below 10 GPa the most stable state is the inverse-spinel magnetite structure (*mag1*) with high-

395   spin Fe and ferrimagnetic ordering between the *OCT* and *TET* sites (Fig. 4). Above 10 GPa, the most stable

396   state is the normal-spinel high-pressure magnetite structure h-Fe_3O_4 with high-spin Fe. This corresponds

397   to an inverse to normal spinel transition due to the phase transition. Within magnetite (*mag1*), there is no

398   inverse to normal spinel transition. The proposed inverse- $\left[Fe^{3+}\right]_{TET}\left[Fe^{2+/3+}Fe^{2+/3+}\right]_{OCT}$ to normal-

399    $\left[Fe^{2+}\right]_{TET}\left[Fe^{3+}Fe^{3+}\right]_{OCT}$ spinel transition in magnetite around 8-15 GPa [15,16] was not supported by the

400   calculations (Fig. 3). As illustrated in the previous figures, there are no spin transitions in inverse-spinel

401   or normal-spinel magnetite or h-Fe_3O_4 as a function of pressure. Across the phase transition the volume

402   decreases by 7-8%, consistent with experimentally measured volume changes (Fig. 5). In magnetite, the

403   calculated volume is almost 4% higher than the experimental values at all pressures (Fig. 5). The

404   discrepancy is consistent with typical volume overestimation of a few percent from GGA vs. experiment.

405   However, some of the error may come from comparing the *Imma* structure of this study, which has charge

406   ordering on the octahedral site, to the $Fd\overline{3}m$ structure[17], which is charge-averaged. The ordering on the

407   octahedral site of *Imma* may expand the lattice relative to the charge-averaged structure ($Fd\overline{3}m$). In h-

408   Fe_3O_4, the computational volume is less than 3% larger the experimental volume (Fig. 5), also consistent

409   with GGA simulations overestimating the volume. A full structural comparison between this study and

410   literature values is given in the supplemental materials[29].

411   The system also undergoes an insulating to metal transition, which can be seen in the electronic

412   density of states (DOS) show in Figure 6. Magnetite (charge ordered, *Imma*) is insulating at the ground

413   state with a band gap of just under 0.2 eV at 0 GPa, consistent with previous computational and

414   experimental studies[30]. Magnetite remains insulating up to 21 GPa. However h-Fe_3O_4 exhibits metallic

415   behavior, with a significant DOS at the Fermi level at 20 GPa.

416   E. Bulk elastic properties as a function of pressure

417   The equation of state parameters were calculated for Fe_3O_4 (Table VII). The calculated bulk

418   modulus, B_0, of inverse- and normal-spinel magnetite vary by less than 5 GPa, and are more compressible

419   than h-Fe_3O_4 by over 15 GPa. Likewise, the volumes of inverse and normal spinel are similar to each

420   other and larger than V_0 of h-Fe_3O_4 by almost 0.9 Å^3/atom. For all cases, lowering the spin state from

421   high-spin to intermediate- and low-spin raises E_0 and lowers V_0. B' remains almost unchanged for lower-

422   spin states. In magnetite, B_0 and B' are in the same range as other experimental and computational values

423   (Table VII). As explained above, the calculated V_0 is ~ 4% larger than the one obtained from experiments.

424

425   **Table VII:** Equation of state parameters for Fe_3O_4 at ambient pressure. Energy, E_0, bulk modulus, B_0, the pressure
426   derivative of the bulk modulus, B', and the ground state volume, V_0, come from fits to a 3rd order Birch-Murnaghan
427   equation of state. Parameters are given for high-spin (HS), intermediate-spin (IS) and low-spin (LS) Fe.

Magnetite: inverse-spinel

	HS	Literature (HS)	IS 2+ OCT	LS 2+ OCT
E_0 (eV/atom)	-6.946		-6.802	-6.774
B_0 (GPa)	173	141-222[17], 180.6[16]	188	172
B'	3.97	4-7.5[17], 4.33[16]	3.98	3.92
V_0 (Å^3/atom)	11.07	10.57[16]	10.78	10.76

h-Fe_3O_4

	HS	IS 2+ TET	LS
E_0 (eV/atom)	-6.888	-6.7506	-
B_0 (GPa)	189	187	-
B'	4.02	3.9974	-
V_0 (Å^3/atom)	10.19	10.1516	-

428

Magnetite: normal spinel

	HS	IS 2+ TET	LS 2+ TET
E_0 (eV/atom)	-6.833	-6.596	-
B_0 (GPa)	169	170	-
B'	3.83	3.89	-
V_0 (Å^3/atom)	11.21	11.02	-

429
430

431

432

IV. DISCUSSION

434   The calculations of the magnetic ordering in inverse-spinel magnetite indicate that there is

435 ferrimagnetic ordering between the *TET* and *OCT* sites $\left[-Fe^{3+}_{HS}-Fe^{3+}_{HS}\right]_{TET}\left[Fe^{3+}_{HS}Fe^{2+}_{HS}Fe^{2+}_{HS}Fe^{3+}_{HS}\right]_{OCT}$ with

436 a residual moment of $8\mu_B$/14-atom unit cell ($4\mu_B$/formula unit). All possible magnetic ordering

437 arrangements in the 14-atom cell were calculated. We confirm that the inverse spinel ordering,

438 $\left[-Fe^{3+}_{HS}-Fe^{3+}_{HS}\right]_{TET}\left[Fe^{3+}_{HS}Fe^{2+}_{HS}Fe^{2+}_{HS}Fe^{3+}_{HS}\right]_{OCT}$, is still the most stable magnetic ordering configuration up

439 to 45 GPa. The computational results therefore suggest that the reduction of total moment by one half

440 observed experimentally[7] cannot be attributed to a change of magnetic ordering arrangements.

441   Having the correct magnetic arrangement at ambient pressure allowed for studying the spin in the

442 correct structure. In our study, we accounted for Fe in different sites (TET and OCT), Fe with different

443 valence (Fe^{2+} and Fe^{3+}), and different charge coordination (inverse spinel and normal spinel). Iron

444 remained high-spin for all charge sets, site occupations, pressures and structures considered. In the

445 calculations, there is no pressure-induced transition from inverse-spinel magnetite to normal-spinel

446 magnetite. The calculations predict a pressure-induced phase transition from inverse-spinel magnetite to

447 normal-spinel h-Fe_3O_4 at 10 GPa, in agreement with some older experimental measurements [17-19] but

448 contradictory to more recent experiments [4,20]. Instead of finding a phase transition, Baudelet et al (2010)

449 and Glazyrin et al (2012) found the magnetic moment decreases with increasing pressure.

450   The high-pressure h-Fe_3O_4 phase is predicted to be antiferromagnetic, but the enthalpies of all

451 magnetic ordering arrangements considered are within 0.175 eV/f.u. of each other. The close energetics

452 are in contrast with inverse-spinel magnetite where magnetic orderings vary by over 0.875 eV/f.u..

453 Therefore, magnetic ordering has a much greater stabilizing effect in inverse-spinel magnetite than in h-

454 Fe_3O_4. The small energy difference between different magnetic arrangements in h-Fe_3O_4 may explain why

455 it has been measured as being paramagnetic at room temperature[17]. The h-Fe_3O_4 phase also remains high-

456 spin for pressures up to 45 GPa (the highest of this study). Therefore, the calculations predict that Fe_3O_4

457 will undergo a phase transition at 10 GPa but the spin state of Fe will remain high-spin for all pressures.

458 **Table VIII:** The magnitudes of the magnetic, $T\Sigma_{magnetic}=kT\ln(2S+1)$, and electronic, $T\Sigma_{electronic}=kT\ln(D)$, entropy
459 contributions to the free energy for high-spin ($3t_{2g}\uparrow2e_g\uparrow t_{2g}\downarrow$), intermediate-spin ($3t_{2g}\uparrow1e_g\uparrow2t_{2g}\downarrow$) and low-spin
460 ($3t_{2g}\uparrow3t_{2g}\downarrow$) Fe^{2+}. S_σ is the spin number and D is the electron degeneracy in t_{2g} and e_g. At room temperature, kT is
461 approximately 0.026 eV. There are 3 Fe atoms in a formula unit of Fe_3O_4, therefore $\Sigma_{magnetic} + \Sigma_{electronic}$ is reported
462 for 3 Fe atoms. The expression for $\Sigma_{magnetic}$ above is only applicable to paramagnets. If magnetite (high-spin Fe) has
463 strong magnetic ordering, there will be no magnetic entropy term ($T\Sigma_{magnetic}=0$). We assume the other phases are
464 paramagnetic. Assuming magnetite with intermediate-spin Fe is paramagnetic provides an upper bound on its free
465 energy gain associated with the magnetic degrees of freedom. The total contribution to the free energy is given by -
466 $T\Sigma_{total}$.

	S_σ	D		$T\Sigma_{magnetic}$ (kT/f.u.)	$T\Sigma_{electronic}$ (kT/f.u.)	$T\Sigma_{total} =$ $T\Sigma_{magnetic} +$ $T\Sigma_{electronic}$ (kT/f.u.)	$-T\Sigma_{total}$ (eV/f.u. at room temp)
High Spin Fe^{2+}	2	3 t_{2g}	Magnetite (magnetically ordered)	0	$3kT\ln(3)$	$3kT\ln(3)$	-0.086
			Magnetite (paramagnetic)	$3kT\ln(5)$	$3kT\ln(3)$	$3kT(\ln(15)$	-0.211
			h-Fe_3O_4	$3kT\ln(5)$	$3kT\ln(3)$	$3kT(\ln(15)$	-0.211
Intermediate Spin Fe^{2+}	1	3 t_{2g}, 2 e_g (total = 3×2 = 6)	magnetite	$3kT\ln(3)$	$3kT\ln(6)$	$3kT(\ln(18))$	-0.225
			h-Fe_3O_4	$3kT\ln(3)$	$3kT\ln(6)$	$3kT(\ln(18))$	-0.225
Low Spin Fe^{2+}	0	1 t_{2g}	magnetite	$3kT\ln(1)$	$3kT\ln(1)$	0	-0.000
			h-Fe_3O_4	$3kT\ln(1)$	$3kT\ln(1)$	0	-0.000

467
468   DFT calculations are effectively at absolute zero and therefore do not include temperature effects.

469 From the DFT calculations alone, it is not clear if increasing temperature could stabilize intermediate-spin

470 with respect to high-spin. The effect of temperature on the spin transition can be determined from the

471 Gibbs free energy expression ($G=H-T\Sigma$). The Gibbs free energy is the sum of the enthalpy, H, and

472 entropy, Σ, (vibrational, magnetic, electronic) terms multiplied by temperature, T. The enthalpy was

473 calculated from DFT (see results section). The entropic terms relevant to spin are the magnetic and

474 electronic entropies estimated for a paramagnetic phase as:

475
$$\Sigma_{magnetic} = k\ln(2S_\sigma + 1)$$
$$\Sigma_{electronic} = k\ln(D)$$

24

476   where S_σ is the spin quantum number, D is the orbital degeneracy in t_{2g} and e_g states, and k is the

477   Boltzmann constant. S_σ and D values for high-, intermediate, and low-spin Fe^{2+} and Fe^{3+} in *OCT* and *TET*

478   sites are shown in Table VIII, where D value are estimated from crystal field arguments [31]. The entropy

479   contributions to the free energy in units of kT ($kT = 0.026$ eV) evaluated at room temperature are given in

480   Table VIII. These estimates assume all phases are paramagnetic except for high-spin magnetite, which is

481   known to have strong magnetic ordering at room temperature. This approach gives the largest possible

482   temperature dependence to the free energy estimates and therefore provides an upper bound on the

483   magnetic and electronic contributions to the spin and phase stability. In magnetite, the sum of the

484   magnetic and electronic contributions to the entropy are -0.086 eV/f.u. for high-spin Fe^{2+}, -0.225 eV/f.u.

485   for intermediate-spin Fe^{2+}, and 0 eV/f.u. for low-spin Fe^{2+} (at room temperature). These additional

486   contributions to the free energy form the electronic and magnetic entropy will only reduce ΔH by 0.139

487   eV/f.u. at room temperature (0.463 eV/f.u. at 1000 K), which is too small to stabilize intermediate-spin

488   (Fig. 2(b)).

489   The effect of temperature and the electronic and spin degrees of freedom on the phase transition

490   from magnetite to h-Fe_3O_4 (Fig. 4b) can also be estimated using the same arguments as above. At room

491   temperature, magnetite with high-spin Fe^{2+} has strong magnetic ordering (Fig. 2a) and thus no magnetic

492   entropy contribution; therefore the entropic and temperature contributions to Gibbs free energy due to

493   high-spin Fe^{2+} is -0.086 eV/f.u.. The high-pressure phase h-Fe_3O_4 has weak magnetic ordering (Fig. 4(a))

494   (paramagnetic, Table VIII) leading to a total contribution to the Gibbs free energy of -0.211 eV/f.u..

495   Thus, temperature will drive the phase transition towards lower pressures and reduce ΔH by 0.125 eV/f.u.

496   (at 300K). If h-Fe_3O_4 retains magnetic ordering, then the entropy contributions to the Gibbs free energy

497   will be the same for magnetite and h-Fe_3O_4 and the phase transition will remain unchanged.

498   It should be noted that there are also vibrational contributions to the free energies of the different

499   phases and spin states in this study. However, we assume that the change in vibrational free energy

500   between different spin states is small due to the general similarity of the structures involved.

501   Furthermore, we expect that lower spin states will produce smaller volumes and correspondingly stiffer

502   lattices, which will reduce the stabilizing effects of vibrational degrees of freedom [32]. Therefore, it is

503   expected that a rigorous treatment of vibrational contributions will only further destabilize the

504   intermediate- and low-spin states. The vibrational contributions to the magnetite to h-Fe_3O_4 transition are

505   not clear; however, because the high-pressure phase is stiffer, it is expected to be destabilized by

506   vibrational contributions, leading to some lowering of the phase transition pressure with increasing

507   temperature.

508   Magnetite is now the third system in which experimental X-ray emission spectra (XES)

509   measurements have been interpreted as intermediate-spin Fe but theoretical calculations have not found

510   intermediate-spin to be stable. In the other systems, $(Mg,Fe)SiO_3$ perovskite and post-perovskite, XES

511   measurements show a drop in peak intensity to a non-zero value, which is interpreted as intermediate spin

512   [8,33]. Yet calculations in perovskite do not predict IS Fe to be stable [9,13,34]. In magnetite, perovskite and

513   post-perovskite, the satellite peak from the XES measurements did not completely disappear. In systems

514   where XES measurements show a drop in satellite peak intensity to zero good agreement exists between

515   theory and XES measurement interpretations. For example, both theory and XES measurements support a

516   high- to low-spin transition in $(Mg,Fe)O$ ferropericlase, (see [35] and references within) and FeS [11].

517   There are two implications of this experimental-theoretical discrepancy. The first is a possible a

518   limitation in the *ab initio* methods. To test this hypothesis, two additional quantum mechanical

519   approaches were used. $DMol^3$, a DFT approach with localized-basis function methods [12], was chosen to

520   test if the localized basis functions of $DMol^3$ better describe intermediate-spin Fe than the planewave

521   basis functions use in VASP. VASP hybrid DFT-Hartree Fock methods [36] were also explored to see if the

522   addition of Hartree-Fock terms to the energetics changed the qualitative predictions regarding

523   intermediate spin. The energy of magnetite was calculated with both methods for high-, intermediate- and

524   low-spin Fe^{2+} on the OCT site[29]. All approaches predict that the OCT Fe^{2+} will remain high-spin up to 40

525   GPa (Table A1). DFT using planewaves and local basis functions, as well as hybrid DFT- Hartree-Fock

526   methods all find high-spin Fe to be stable with respect to intermediate-spin Fe. Cluster-based DFT

527   methods with newer functionals do not find a stable intermediate-spin state in perovskite[13] and other iron-

528 bearing complexes either[37]. The agreement amongst these various methods suggests the calculations are

529 capturing the correct spin behavior of iron, however the small possibility exists that essential physics of

530 intermediate-spin are not accurately described.

531   The more plausible implication of the experimental-theoretical discrepancy is that the observed

532 drop of satellite peak intensity to a non-zero value in XES measurements at high-pressure is due to a

533 change other than a transition to intermediate-spin iron, such as electron delocalization with pressure [4,20].

534 If XES with a satellite peak that is reduced to a non-zero value cannot be interpreted as intermediate-spin

535 Fe^{2+}, then Fe^{2+} in magnetite, perovskite, and post-perovskite will remain high-spin.

536

537

V. CONCLUSIONS

The *ab initio* calculations isolated the complex magnetic ordering, valence states, charge ordering, and different local Fe site environments in magnetite and h-Fe_3O_4 as a function of pressure. The calculations found a pressure-induced structural phase transition from inverse-spinel magnetite to normal spinel h-Fe_3O_4. The magnetic ordering of inverse-spinel magnetite does not change with pressure and iron remains high-spin for all pressures. There is no evidence from the *ab initio* energetics for an inverse to normal spinel transition with pressure in magnetite. However, the magnetite to high-pressure magnetite h-Fe_3O_4 phase transition corresponds to an inverse to normal spinel transition, but the normal-spinel h-Fe_3O_4 has a different symmetry and structure from magnetite.

The most stable spin state is high-spin Fe in the ferrimagnetic arrangement for both magnetite and high-pressure magnetite h-Fe_3O_4 structures up to 50 GPa (the highest pressure considered in this study). The calculations have accounted for site occupation, valence, and charge coordination. Intermediate-spin iron is not stable in magnetite, contrary to experimental measurements[7]. The discrepancy between theoretical and experimental measurements of intermediate-spin iron only occurs when the x-ray emission spectra satellite peak intensity drops to a non-zero value, which has been seen in magnetite, perovskite, and post-perovskite. The results suggest *X*-ray emission spectra may need to be interpreted differently at high pressures. Failure to find intermediate spin in magnetite implies Fe^{2+} in perovskite and post perosvkite will also remain high spin.

567   **Figure 1:** (a) magnetite. As inverse spinel, the octahedral site (OCT, light grey) is a statistical distribution of Fe^{2+} and
568   Fe^{3+} and the tetrahedral site (TET, black) is Fe^{3+}. As normal spinel, the octahedral site is Fe^{3+} and the tetrahedral site
569   is Fe^{2+}. (b) h-Fe_3O_4, the high-pressure magnetite phase. The octahedral site (OCT, light grey) is Fe^{3+} and the
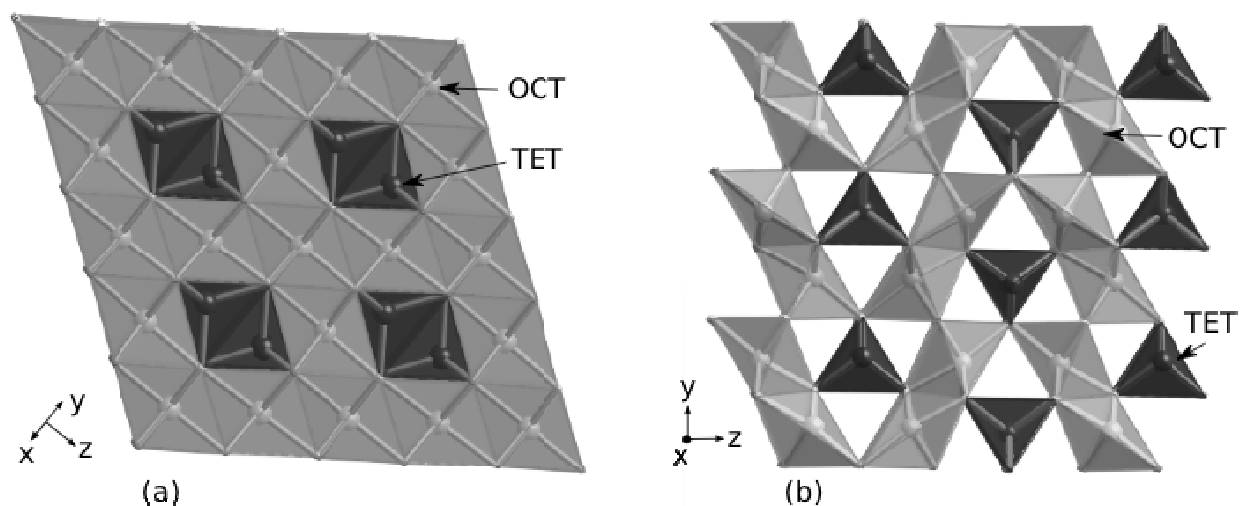570   tetrahedral site (TET, black) is Fe^{2+}.

(a)   (b)

571
572
573
574

30

575 **Figure 2:** (a) stable magnetic ordering in inverse-spinel magnetite. All enthalpies are referenced to high-spin (HS)
576 magnetite, *mag1*. Abbreviations are explained in Table III. (b) Spin states in inverse spinel magnetite. Enthalpies of
577 Fe^{2+} in high-, intermediate- (IS), and low-spin (LS) states on the octahedral (*OCT*) site referenced to high-spin
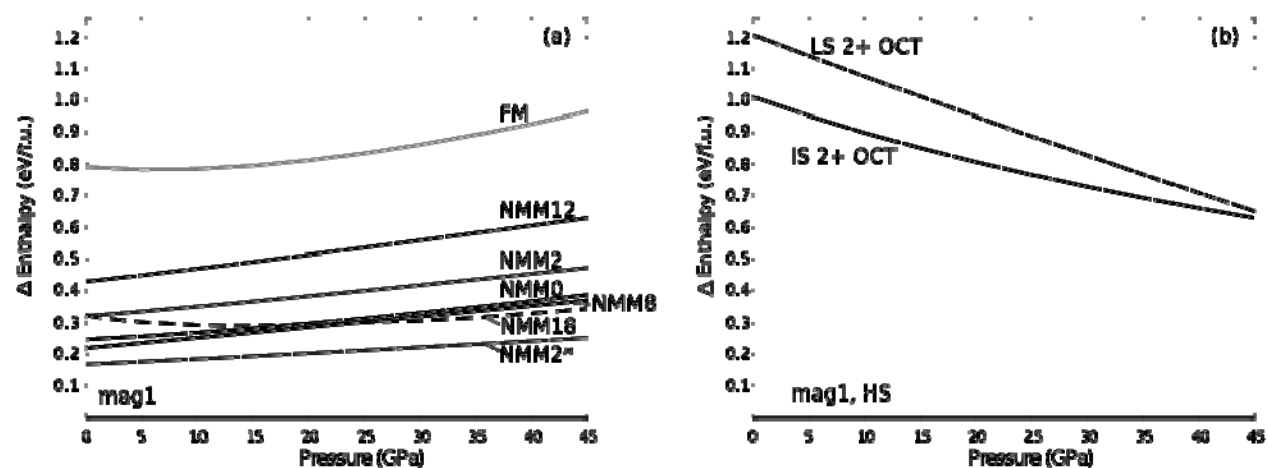578 magnetite. Abbreviations are explained in Table IV.
579

580
581
582

583 **Figure 3:** stable spin states in normal-spinel magnetite. All enthalpies are referenced to HS magnetite with the
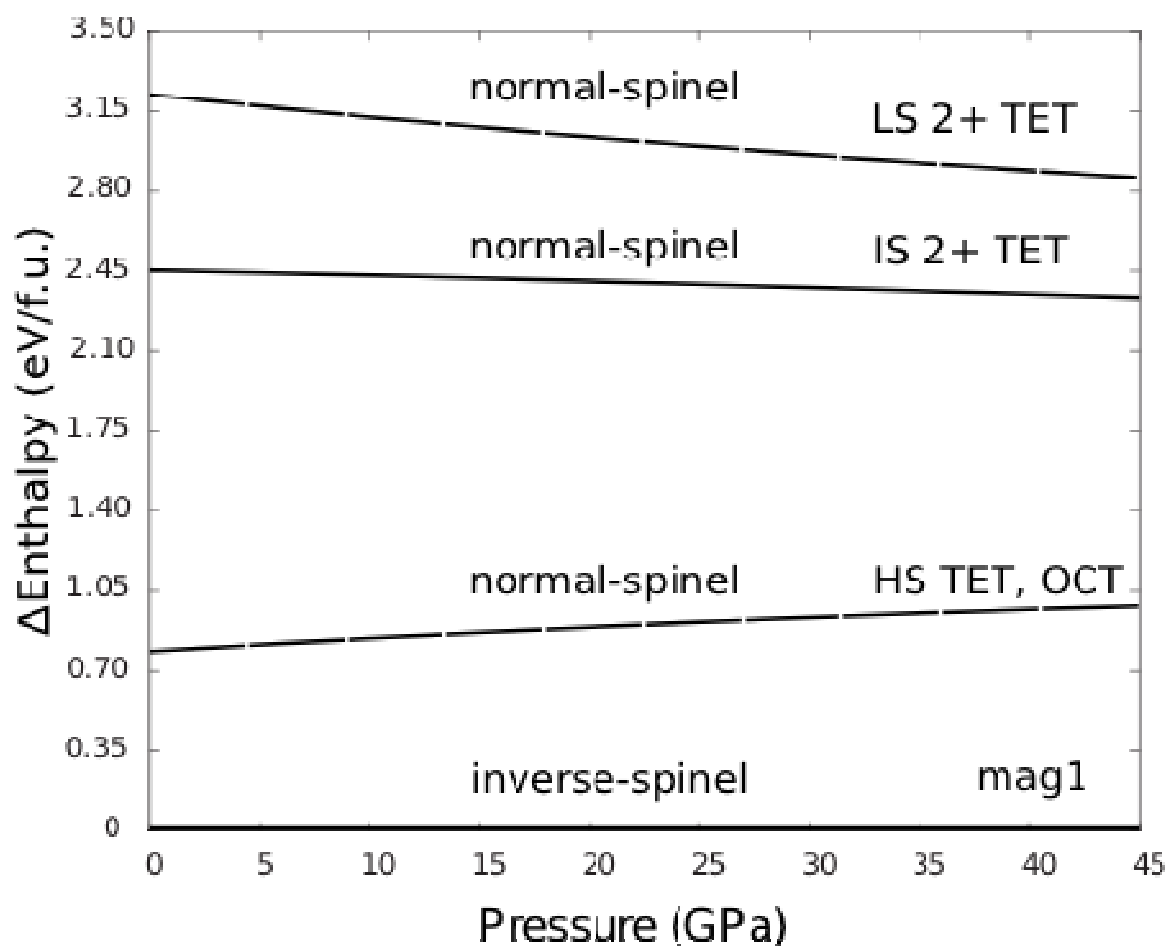584 inverse spinel structure, *mag1*. Details of the magnetic arrangements can be found in Table V.

585
586
587

588 **Figure 4:** (a) Stable magnetic arrangements in normal-spinel h-Fe_3O_4 referenced to high-spin magnetite, *mag1* (b)
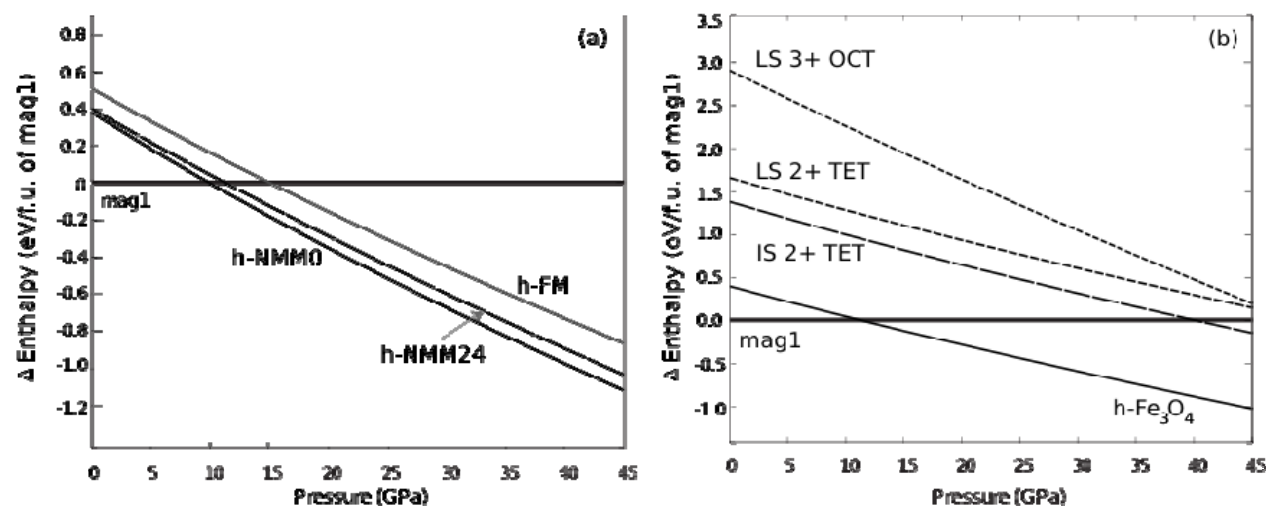589 Stable spin states in h-Fe_3O_4 *Pbcm*. Abbreviations for spin states and magnetic orderings given in Table VI.
590

591
592
593

594 **Figure 5:** Volume change across phase transition from inverse-spinel magnetite (

595 $\left[-Fe_{HS}^{3+} - Fe_{HS}^{3+}\right]_{TET}\left[Fe_{HS}^{3+}Fe_{HS}^{2+}Fe_{HS}^{2+}Fe_{HS}^{3+}\right]_{OCT}$) to h-$Fe_3O_4$ ($\left[-Fe^{2+}\right]_{TET}\left[Fe^{3+}Fe^{3+}\right]_{OCT}$). The volume curves

596 for each phase are given in orange squares (light for magnetite, dark for h-Fe_3O_4). The dashed orange line follows

597 the stable phase as a function of pressure. Experimental volumes for magnetite and h-Fe_3O_4 (grey/black circles[17]) are

598 shown for comparison with the calculations. The dashed black line follows the experimental stable phase as a
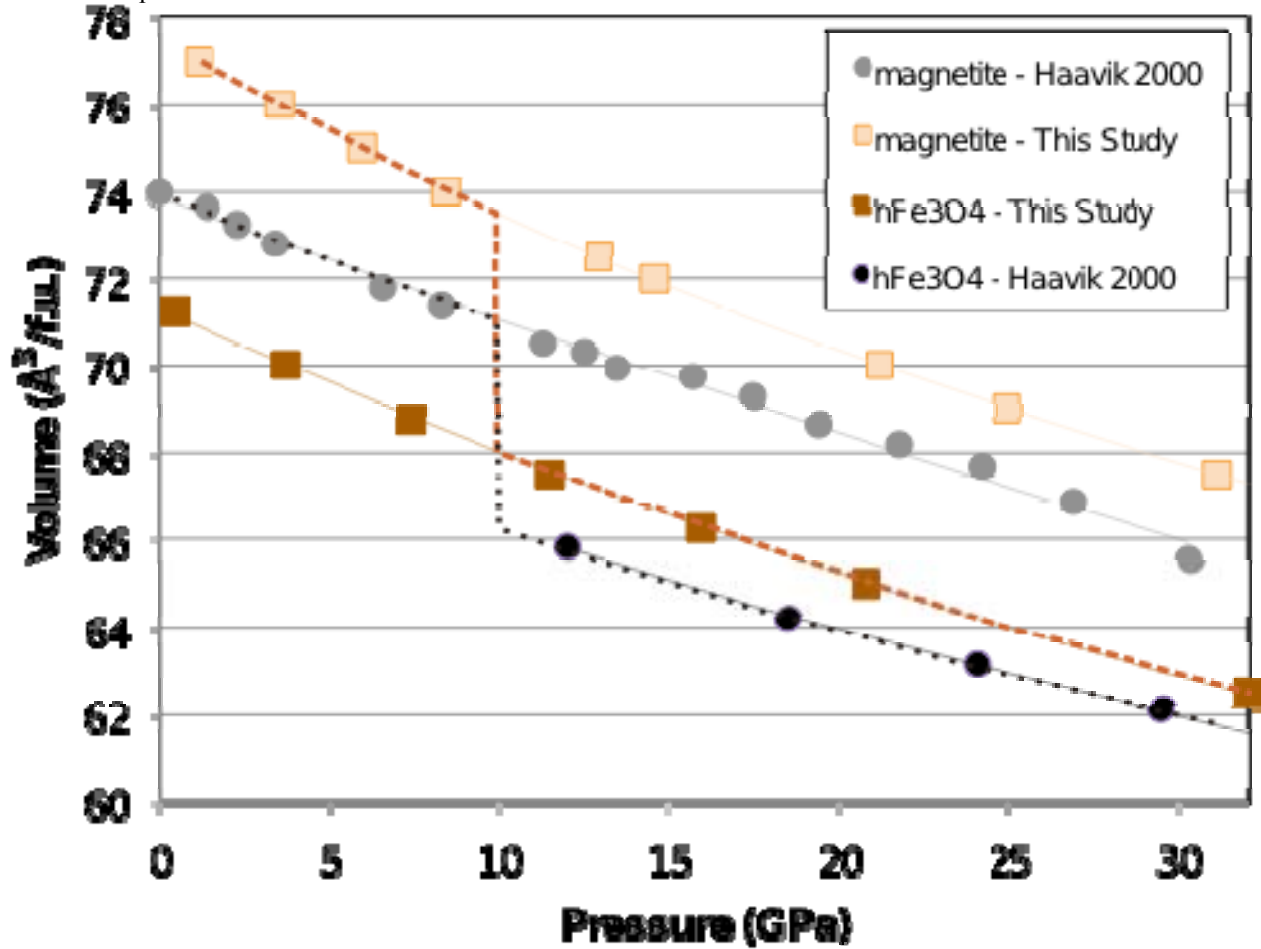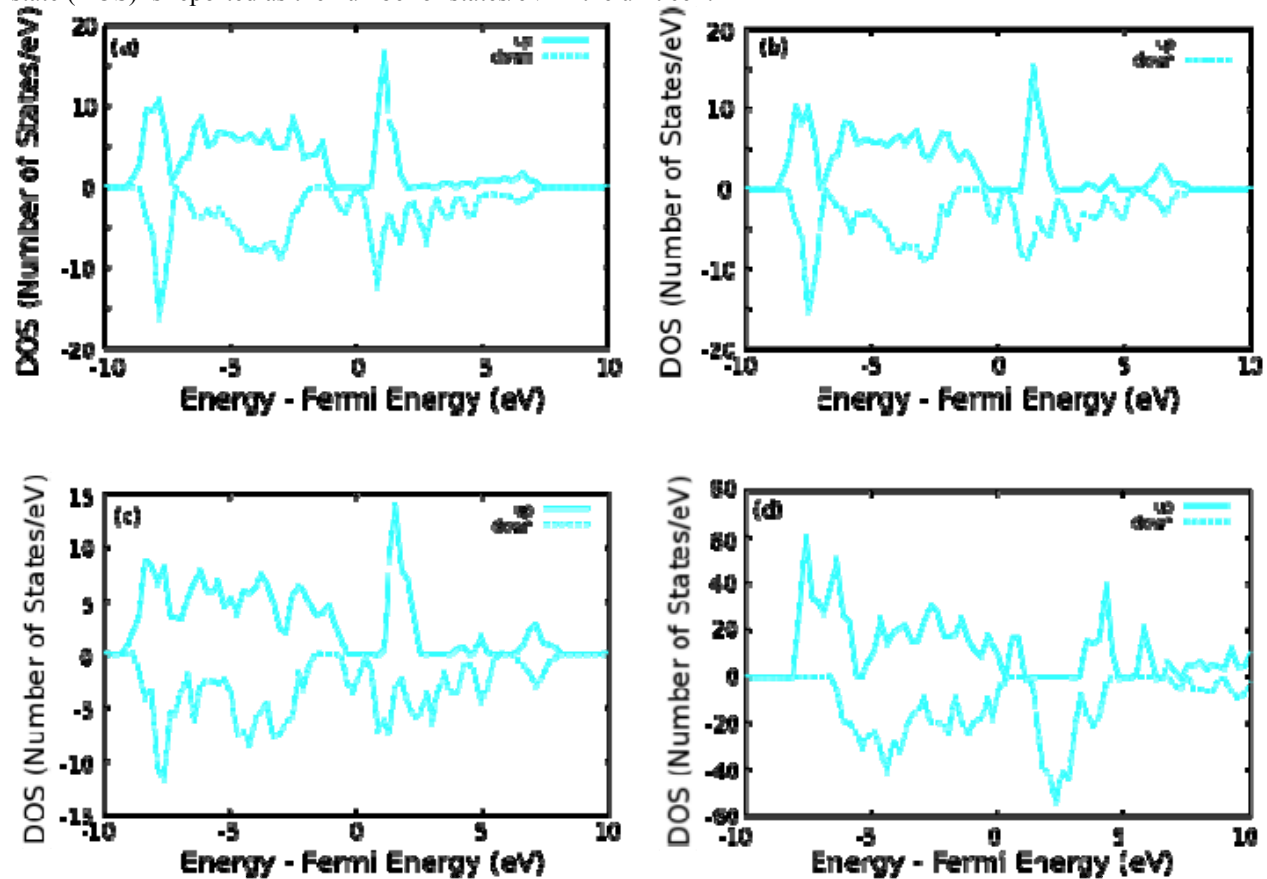
599 function of pressure

600
601

602 **Figure 6:** Electronic structure of (a) magnetite, $\left[-Fe^{3+}_{HS}-Fe^{3+}_{HS}\right]_{TET}\left[Fe^{3+}_{HS}Fe^{2+}_{HS}Fe^{2+}_{HS}Fe^{3+}_{HS}\right]_{OCT}$, at ambient

603 pressure (b) magnetite at 1 GPa, (c) magnetite at 21.1 GPa, and (d) h-Fe3O4, $\left[-Fe^{2+}\right]_{TET}\left[Fe^{3+}Fe^{3+}\right]_{OCT}$, at 20.8

604 GPa with high-spin Fe on all sites. The Fermi energy has been subtracted from all energy values. The density of
605 state (DOS) is reported as the number of states/eV in the unit cell.

606
607
608
609
610
611
612

References

1   D. J. Dunlop and O. Özdemir, *Rock Magnetism: Fundamentals and frontiers*. (Cambridge University Press, Cambridge, 1997), 1st edition ed.

2   P. E. van Keken, Earth Planet. Sci. Lett. **215** (2003).

3   D. I. Gough, Earth-Science Reviews **32**, 3 (1992).

4   K. Glazyrin, C. McCammon, L. Dubrovinsky, M. Merlini, K. Schollenbruch, A. Woodland, and M. Hanfland, Am. Miner. **97**, 128 (2012).

5   J. F. Lin and T. Tsuchiya, Phys. Earth Planet. Inter. **170**, 248 (2008).

6   M. Dolg, U. Wedig, H. Stoll, and H. Preuss, J. Chem. Phys. **86**, 866 (1987).

7   Y. Ding, D. Haskel, S. G. Ovchinnikov, Y. C. Tseng, Y. S. Orlov, J. C. Lang, and H. K. Mao, Phys. Rev. Lett. **100**, 045508 (2008).

8   C. McCammon, I. Kantor, O. Narygina, J. Rouquette, U. Ponkratz, I. Sergueev, M. Mezouar, V. Prakapenka, and L. Dubrovinsky, Nature Geosci. **1**, 684 (2008); Jung-Fu Lin, Heather Watson, Gyorgy Vanko, Esen E. Alp, Vitali B. Prakapenka, Przemek Dera, Viktor V. Struzhkin, Atsushi Kubo, Jiyong Zhao, Catherine McCammon, and William J. Evans, Nature Geosci. **1**, 688 (2008).

9   A. Bengtson, J. Li, and D. Morgan, Geophys. Res. Lett. **36**, L15301 (2009); Han Hsu, Koichiro Umemoto, Peter Blaha, and Renata M. Wentzcovitch, Earth Planet. Sci. Lett. **294**, 19 (2010).

10   V. I. Anisimov, F. Aryasetiawan, and A. I. Lichtenstein, J. Phys.-Condes. Matter **9** (1997).

11   R. S. Kumar, Y. Zhang, Y. M. Xiao, J. Baker, A. Cornelius, S. Veeramalai, P. Chow, C. F. Chen, and Y. S. Zhao, Appl. Phys. Lett. **99**, 061913 (2011).

12   B. Delley, J. Chem. Phys. **92**, 508 (1990).

13   James R. Rustad and Qing-Zhu Yin, Nature Geosci. **advanced online publication**, 14 June 2009. DOI: 10.1038/NGEO546 (2009).

14   E. J. W. Verwey, Nature **144**, 327 (1939).

15   M. P. Pasternak, W. M. Xu, G. K. Rozenberg, R. D. Taylor, and R. Jeanloz, **65** (2004).

16   G. K. Rozenberg, Y. Amiel, W. M. Xu, M. P. Pasternak, R. Jeanloz, M. Hanfland, and R. D. Taylor, Phys. Rev. B **75**, 020102 (2007).

17   C. Haavik, S. Stolen, H. Fjellvag, M. Hanfland, and D. Hausermann, Am. Mineral. **85**, 514 (2000).

18   Y. W. Fei, D. J. Frost, H. K. Mao, C. T. Prewitt, and D. Hausermann, Am. Mineral. **84**, 203 (1999).

646   19   L. S. Dubrovinsky, N. A. Dubrovinskaia, C. McCammon, G. K. Rozenberg, R. Ahuja, J. M.
647   Osorio-Guillen, V. Dmitriev, H. P. Weber, T. Le Bihan, and B. Johansson, **15** (2003).

648   20   F. Baudelet, S. Pascarelli, O. Mathon, J. P. Itie, A. Polian, and J. C. Chervin, Phys. Rev. B **82**,
649   140412 (2010).

650   21   G. Kresse and J. Furthmuller, Comput. Mater. Sci. **6**, 15 (1996); G. Kresse and J. Furthmuller,
651   Phys. Rev. B **54**, 11169 (1996); G. Kresse and J. Hafner, Phys. Rev. B **47**, 558 (1993).

652   22   G. Kresse and D. Joubert, Phys. Rev. B **59**, 1758 (1999);   P. E. Blochl, Phys. Rev. B **50**,
653   17953 (1994).

654   23   J. P. Perdew, K. Burke, and M. Ernzerhof, Phys. Rev. Lett. **77**, 3865 (1996).

655   24   M. J. Wenzel and G. Steinle-Neumann, Phys. Rev. B **75**, 214430 (2007).

656   25   A. I. Liechtenstein, V. I. Anisimov, and J. Zaanen, **52** (1995).

657   26   E. Nazarenko, J. E. Lorenzo, Y. Joly, J. L. Hodeau, D. Mannix, and C. Marin, Phys. Rev. Lett.
658   **97**, 056403 (2006).

659   27   J. P. Wright, J. P. Attfield, and P. G. Radaelli, Phys. Rev. B **66**, 214422 (2002).

660   28   M. E. Fleet, Acta Crystallogr. Sect. B-Struct. Commun. **37**, 917 (1981).

661   29   additinal structural details See Supplemental Material at [URL will be inserted by publisher] for
662   details on atomic positions, a comparison of h-Fe3O4 space groups, other computational
663   methods, the Hubbard-U dependence and computational relaxation choices.

664   30   P. Piekarz, K. Parlinski, and A. M. Oles, Phys. Rev. Lett. **97**, 156402 (2006).

665   31   R. G. Burns, *Mineralogical applications of crystal field theory*. (Cambridge University Press,
666   1993).

667   32   A. van de Walle and G. Ceder, Rev. of Mod. Phys. **74**, 11 (2002).

668   33   J. Li, V. V. Struzhkin, H. K. Mao, J. F. Shu, R. J. Hemley, Y. W. Fei, B. Mysen, P. Dera, V.
669   Prakapenka, and G. Y. Shen, Proc. Natl. Acad. Sci. U. S. A. **101**, 14027 (2004).

670   34   A. Bengtson, K. Persson, and D. Morgan, Earth Planet. Sci. Lett. **265**, 535 (2008).

671   35   K. Persson, A. Bengtson, G. Ceder, and D. Morgan, Geophys. Res. Lett. **33**, L16306 (2006).

672   36   A. V. Krukau, O. A. Vydrov, A. F. Izmaylov, and G. E. Scuseria, J. Chem. Phys. **125**, 224106
673   (2006).

674   37   M. Swart, J. Chem. Theory Comput. **4**, 2057 (2008).

675   38   T. Kawakami, Y. Tsujimoto, H. Kageyama, X. Q. Chen, C. L. Fu, C. Tassel, A. Kitada, S. Suto,
676   K. Hirama, Y. Sekiya, Y. Makino, T. Okada, T. Yagi, N. Hayashi, K. Yoshimura, S. Nasu, R.
677   Podloucky, and M. Takano, Nature Chem. **1**, 371 (2009).

678   39   A. Bergner, M. Dolg, W. Kuchle, H. Stoll, and H. Preuss, Mol. Phys. **80**, 1431 (1993).

679   40   Nathan Pinney, James D. Kubicki, Derek S. Middlemiss, Clare P. Grey, and Dane Morgan,
680   Chemistry of Materials **21**, 5727 (2009).

681   41   T. Tsuchiya, R. M. Wentzcovitch, C. R. S. da Silva, S. de Gironeoli, and J. Tsuchiya, Phys. Status
682   Solidi B-Basic Solid State Phys. **243**, 2111 (2006).
683
684
685

686
687
688

689
690
691
692
693
694
695